Coupled Systems Mechanics, *Vol. 15, No. 1 (2026) 1-16*
https://doi.org/10.12989/csm.2026.15.1.001

Techno-Press

Aluminum-wooden beam bonded by carbon fiber reinforced polymer: analysis and modeling

Tahar Hassaine Daouadji*[1,2], Belkacem Adim[1,3,4], Ayed Eid Alluqmani[5], Bensatallah Tayeb[1,2]

[1]*Laboratory of Geomatics and Sustainable Development, University of Tiaret, Algeria*
[2]*Department of Civil Engineering, Ibn Khaldoun University of Tiaret, Algeria*
[3]*Department of Civil, Mechanical and Transportation Engineering, Tissemsilt University, Algeria*
[4]*Construction Engineering and Materials Sciences Laboratory, Tissemsilt University, Algeria*
[5]*Department of Civil Engineering, Faculty of Engineering, Islamic University of Madinah, Al-Madinah Al-Munawara, Prince Naif Ibn Abdulaziz, Al Jamiah, Medina 42351, Saudi Arabia*

(Received September 1, 2025, Revised December 4, 2025, Accepted January 29, 2026)

Abstract. This article proposes a new type of aluminum-wood composite beam that reduces material weight and enhances lightweight construction. The beam is reinforced by composite material plates, providing additional rigidity. The beam has three cross-sections: I-shape, U-shape, and rectangular tube, with adhesive connection for both interfaces. The interfacial stresses in aluminum-wood composite beams reinforced by composite laminates are analyzed using nonlinear elastic theory and strain compatibility approach. The model considers shear deformations of the interface and is intended to be applied to all types of bonded materials. Theoretical predictions are compared with existing solutions, contributing to understanding the mechanical behavior of the interface and designing aluminum-wood structures reinforced by composite materials.

Keywords: adhesive bonding; aluminum-wooden composite beam; composite plate; interfacial stresses; plate; shear lag effect; slip; strengthening

1. Introduction

Composite structures are recognized for their exceptional performance in the construction sector, attributed to key characteristics such as high stiffness, low weight, excellent ductility, and resilience during seismic events. A vital element in these structures is shear connectors, which play a significant role in linking slabs to beams within composite beams. Despite their importance, shear connectors face challenges under external load conditions, leading to interface slip as a consequence of longitudinal horizontal shear [1-5]. This slip has critical implications, resulting in alterations to the section curvature, an increase in deflection, and a subsequent decrease in both flexural stiffness and load-carrying capacity of the composite beams. Understanding these effects is essential for improving the design and functionality of composite structures in construction. The study aims to reduce slab sliding by using a new bonding technique, ensuring slab-beam connection using adhesive, to reduce this issue [6-15]. The composite aluminum-wood beam

*Corresponding author, Professor, E-mail: daouadjitahar@gmail.com

ISSN: 2234-2184 (Print), 2234-2192 (Online)

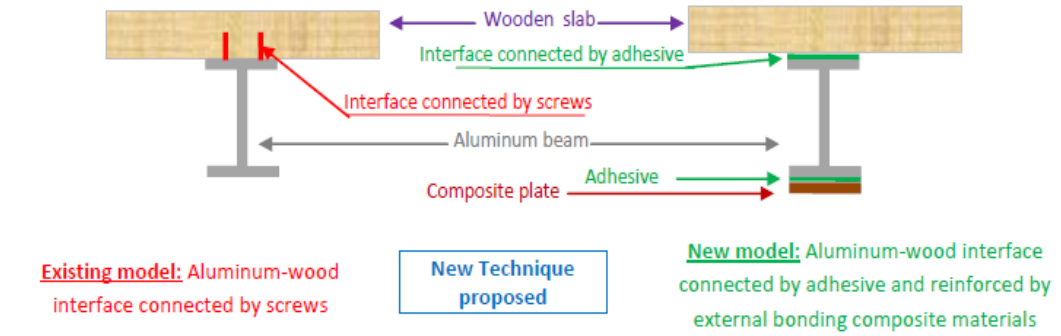

Figure 1. Cross-section view of mechanical connected (existing model) and adhesive bonded (new model) Aluminum-wooden composite beam

member exhibits greater flexibility compared to traditional steel beams and concrete slabs. This enhanced performance, however, is contingent upon the integrity of the connection at the aluminum-wood interface. This connection is crucial as it must withstand applied loads and effectively transfer stresses. The efficiency of the connection is fundamentally linked to the level of interaction between the aluminum and wood components [16-21]. This interaction is specifically assessed through the shear stiffness of the composite connection, which is determined by the relative slip that occurs at the composite interface under load conditions. Based on relative slip, aluminum-wood composite connections can be broadly classified as flexible [22-30].

Construction aims to build structures that can withstand loads and function while also being sustainable and resistant to environmental damage. The objective is to maintain the same level of performance for as long as possible, including load distribution, durability, and aesthetic appearance. If performance drops, the structure must be strengthened, a principle known as renovation. New technology in wood construction is emerging to increase structure resistance, particularly in mixed wooden construction. Wood structures offer several advantages, such as lightweight construction, energy efficiency, environmental sustainability, and aesthetic appeal. With the advent of modern technological advancements, wooden structures have garnered extensive utilization in public constructions, residential buildings, and even towering high-rises. Within such constructions, the floor is crucial in providing support for vertical loads and furnishing resistance against lateral forces. The wood-aluminum composite slab emerges as an innovative variant of the wood slab. It amalgamates wood members and aluminum into a cohesive structure through shear connections, thereby facilitating the utilization of the material properties.

A study on the shear behavior of screw fasteners found that increasing the embedded length in aluminum-wood beams significantly improved their shearing capacity. Other studies investigated the influence of inter-layer board thickness and screw diameter on shear performance in composite beams with interlayer boards. Winkler's elastic foundation beam theory was used to establish a mechanical model for shear stiffness. Research also found that wood type had minimal impact on stud connections' mechanical behavior, while the shear performance of screw connectors primarily depended on the compressive strength parallel to the wood grain. The study compared the behavior of mechanically connected and adhesively bonded aluminum-wooden composite connections under flexural loading (Fig. 1). The effectiveness of the composite connection depends on the degree of interaction between aluminum and wood. Adhesively bonded connections minimized slip, while mechanically connected bonds showed a significant value of

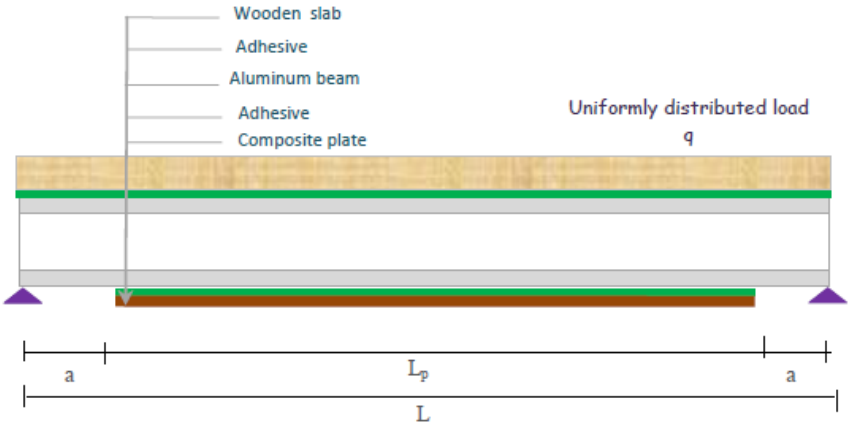

Figure 2. Simply supported composite aluminum-wooden beam strengthened by composite plate

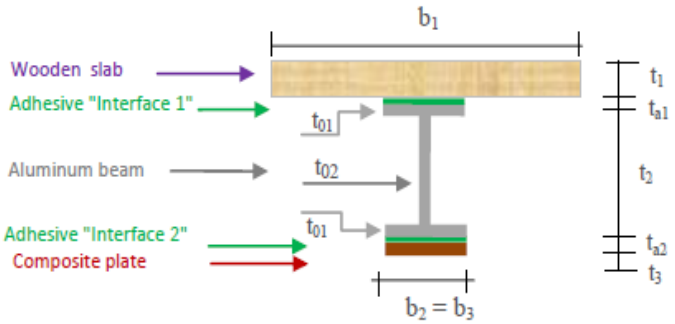

Figure 3. Cross section of a simply supported composite aluminum-wooden beam strengthened by composite plate

steel-concrete slip compared to perfectly bonded bonds.

This study presents analytical studies on developing closed-form solutions for interfacial shear and normal stresses, sliding of wooden slabs, and the strengthening of aluminum structures in situ with externally bonded composite plates. The study presents a closed-form solution for sliding of wooden slabs and interfacial shear stress in a simply supported aluminum-wooden composite beam, subjected to uniformly distributed load. The results are satisfactory compared to literature, demonstrating the potential of this method for repairing aluminum structures in construction. The novelty of this research lies in the aluminum-wooden composite beam coupling, whose connection is ensured by a continuous connection, in this case an adhesive, replacing the previous discontinuous connection of screws or rivets. This new technique is used to modernize aluminum-wooden composite beams, while aiming for application in civil construction.

2. Mathematical formulation of the present method

2.1 Basic assumptions

The analysis considers transverse shear stress and deformation in an aluminum beam and

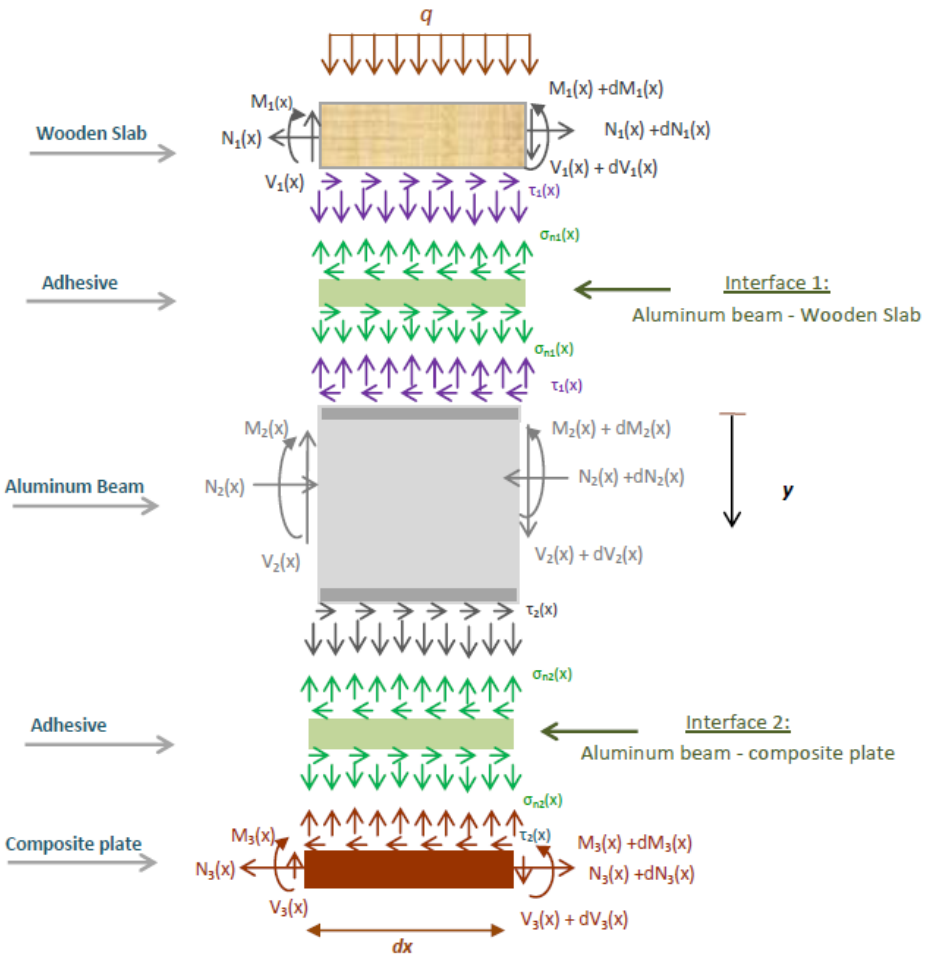

Figure 4. Forces in infinitesimal element of a composite aluminum-wooden beam strengthened by composite plate

wooden slab, comparing it with a literature analysis for a composite aluminum-wood beam strengthened by a composite plate. The study compares the analytical approach from the literature [2, 27] for wooden slabs glued to the beam with composite plates (Figs. 2 and 3).

Hassaine Daouadji [27] propose that the analytical approach is based on certain assumptions.

- Elastic stress strain relationship for aluminum, wooden and adhesive;
- The composite simply supported beam and shallow, i.e., plane sections remain plane in bending.
- There is an imperfect bond between the wooden slab and the aluminum beam; there will be a possibility of sliding between these two members.
- The stresses in the adhesive layer do not change through the direction of the thickness.
- The shear stress analysis assumes that the curvatures in the composite beam and composite plate are equal (since this allows the shear stress and peel stress equations to be uncoupled). However, this assumption is not made in the normal stress solution, i.e., when the beam is loaded, vertical separation occurs between composite wooden beam and composite plate.

The composite aluminum-wood beam, made from four materials: CFRP composite material, wooden, adhesive, and aluminum beam, is analyzed for linear elastic behavior (Fig. 4). All materials must resist forces and moments caused by transverse uniformly distributed loads. Deformations must accommodate interface slip, flexural and axial strains, and accommodate any interface slip in addition to the usual strains. The analysis shows that these deformations must accommodate any interface slip.

2.2 Stress analysis at interface 1: Aluminum beam-wooden slab

2.2.1 Shear stress distribution along the Aluminum beam-wooden slab interface

The governing differential equation for the interfacial shear stress is expressed as [27]:

$$\frac{d^2\tau(x)}{K_s \cdot dx^2} - K_1 b_2 \left[\frac{(y_1+y_2)(y_1+y_2+t_{a1})}{E_1I_1+E_2I_2} + \frac{1}{E_1A_1} + \frac{1}{E_2A_2}\right]\tau(x) + K_1 \frac{(y_1+y_2)}{E_1I_1+E_2I_2} \cdot V_T(x) = 0 \tag{1}$$

Where:

$$K_1 = \left[\frac{t_{a1}}{G_{a1}} + \frac{t_1}{4G_1} + \frac{5t_2}{12G_2}\right]^{-1} \tag{2}$$

For simplicity, the general solutions presented below are limited to loading which is either concentrated or uniformly distributed over part or the whole span of the composite wooden beam, or both. The general solution to Eq. (1) is given by simplified form:

$$\tau(x) = \eta_1 e^{\lambda \cdot x} + \eta_2 e^{-\lambda \cdot x} + \frac{K_1}{\lambda^2}\left(\frac{1}{E_1A_1} + \frac{1}{E_2A_2}\right).V_T(x) \tag{3}$$

$$\tau(x) = \eta_1 e^{\lambda \cdot x} + \eta_2 e^{-\lambda \cdot x} + \delta.V_T(x) \tag{4}$$

Where:

$$\lambda^2 = \left[\frac{b_2(y_1+y_2)(y_1+y_2+t_{a1})}{E_1I_1+E_2I_2} + \frac{b_2}{E_1A_1} + \frac{b_2}{E_2A_2}\right]\left[\frac{t_{a1}}{G_{a1}} + \frac{t_1}{4G_1} + \frac{5t_2}{12G_2}\right]^{-1} \tag{5}$$

And:

$$\delta = \frac{\left(\frac{1}{E_1A_1} + \frac{1}{E_2A_2}\right)}{b_2\left[\frac{(y_1+y_2)(y_1+y_2+t_{a1})}{E_1I_1+E_2I_2} + \frac{1}{E_1A_1} + \frac{1}{E_2A_2}\right]} \tag{6}$$

$$\tau(x) = \eta_1 e^{\lambda \cdot x} + \eta_2 e^{-\lambda \cdot x} + \frac{\left(\frac{1}{E_1A_1} + \frac{1}{E_2A_2}\right)}{b_2\left[\frac{(y_1+y_2)(y_1+y_2+t_{a1})}{E_1I_1+E_2I_2} + \frac{1}{E_1A_1} + \frac{1}{E_2A_2}\right]} V_T(x) \tag{7}$$

η_1 and η_2 are constant coefficients determined from the boundary conditions. The interfacial shear stress for this uniformly distributed load: For $0 \le x \le L_p$ at any point is written as:

$$\tau(x) = \left(\frac{\frac{t_2 a(L-a)}{2E_2 I_2}}{\frac{t_{a1}}{G_{a1}} + \frac{t_1}{4G_1} + \frac{5t_2}{12G_2}} - \frac{(t_1+t_2)}{2\lambda^2(E_2 I_2 + E_1 I_1 + b_1)}\right)\frac{qe^{-\lambda x}}{\lambda} + \frac{t_1+t_2}{2\lambda^2(E_2 I_2 + E_1 I_1 + b_1)} q\left(\frac{L}{2} - a - x\right) \quad (8)$$

Where q is the uniformly distributed load and x; a; L and Lp are defined in Fig. 2

2.2.2 Slip distribution along the Aluminum-wooden slab interface

The following governing differential equation for the slip strain at the interface of uniformly distributed load is calculated as [27]:

$$\frac{dS(x)}{dx} = \frac{du_1(x)}{dx} - \frac{du_2(x)}{dx} = \varepsilon_1(x) - \varepsilon_2(x) \quad (9)$$

As noted in the assumptions, the slip of adhesive is proportional to the shear force, $\tau(x)$ which the connector transmitted. The constant of proportionality is the adhesive stiffness K_{a1}.

The slip stress in the adhesive can be expressed as follows:

$$S(x) = \frac{t_{a1}}{G_{a1}}\left(\eta_1 e^{\lambda \cdot x} + \eta_2 e^{-\lambda \cdot x} + \frac{K_1}{\lambda^2}\left(\frac{1}{E_1 A_1} + \frac{1}{E_2 A_2}\right).V_T(x)\right) \quad (10)$$

Where $S(x)$ represent slip between adhrends and $K_s = \frac{G_{a1}}{t_{a1}}$ is shear stiffness of the adhesive, G_{a1} and t_{a1} are shear modulus and thickness of the adhesive.

2.3 Stress analysis at interface 2: Aluminum beam composite plate-interface

2.3.1 Shear stress distribution along the composite plate-Aluminum beam interface

The governing differential equation for the interfacial shear stress is expressed as [27]:

$$\frac{d^2\tau(x)}{dx^2} - \frac{b_2\left[\frac{(y_2+y_3)(y_2+y_3+t_{a2})}{E_2 I_2 + E_3 I_3} + \frac{1}{E_2 A_2} + \frac{1}{E_3 A_3}\right]}{\frac{t_{a2}}{G_{a2}} + \frac{t_2}{4G_2} + \frac{5t_3}{12G_3}}\tau(x) + \frac{\left[\frac{y_2+y_3}{E_2 I_2 + E_3 I_3}\right]}{\frac{t_{a2}}{G_{a2}} + \frac{t_2}{4G_2} + \frac{5t_3}{12G_3}} V_T(x) = 0 \quad (11)$$

For simplicity, the general solutions presented below are limited to loading which is either concentrated or uniformly distributed over part or the whole span of the beam, or both. For such loading, $d^2V_T(x)/dx^2=0$, and the general solution to Eq. (11) is given by

$$\tau(x) = \eta_7 \cosh(\xi x) + \eta_8 \sinh(\xi x) + \frac{(t_2+t_3)}{2\xi^2\left(\frac{t_{a2}}{G_{a2}} + \frac{t_2}{4G_2} + \frac{5t_3}{12G_3}\right)(E_2 I_2 + E_3 I_3)} V_T(x) \quad (12)$$

Where:

$$\xi = \left[\frac{b_2 \left[\frac{(t_2 + t_3)(t_2 + t_3 + 2t_{a2})}{4(E_2 I_2 + E_3 I_3)} + \frac{1}{E_2 A_2} + \frac{1}{E_3 A_3} \right]}{\frac{t_{a2}}{G_{a2}} + \frac{t_2}{4G_2} + \frac{5t_3}{12G_3}} \right]^{\frac{1}{2}} \tag{13}$$

And η_7 and η_8 are constant coefficients determined from the boundary conditions. In the present study, a simply supported beam has been investigated which is subjected to a uniformly distributed load. For our case of a uniformly distributed load, the formula of the shear stress is given by the following equation:

$$\tau(x) = \left[\frac{1}{\xi} \left(\frac{t_{a2}}{G_{a2}} + \frac{t_2}{4G_2} + \frac{5t_3}{12G_3} \right) \left(\frac{A_{11}^{'}}{b_3} P_0 - \frac{y_2 M_t(0)}{E_2 I_2} \right) \right] e^{-\xi x} + \frac{(t_2 + t_3)(a.q + x - \frac{e^{-\xi x}}{\xi} q)}{2\xi^2 \left(\frac{t_{a2}}{G_{a2}} + \frac{t_2}{4G_2} + \frac{5t_3}{12G_3} \right)(E_2 I_2 + E_3 I_3)} \tag{14}$$

$$0 \le x \le L_p$$

2.3.2 Normal stress distribution along the composite plate-Aluminum beam interface

The following governing differential equation for the interfacial normal stress for this uniformly distributed load [27]:

$$\frac{d^4 \sigma_n(x)}{dx^4} + K_{n2} \left(D_{11}^{'} + \frac{b_3}{E_2 I_2} \right) \sigma_n(x) - K_{n2} \left(D_{11}^{'} \frac{t_3}{2} - \frac{y_2 b_3}{E_2 I_2} \right) \frac{d\tau(x)}{dx} + \frac{q K_{n2}}{E_2 I_2} = 0 \tag{15}$$

Where K_n is the normal stiffness of the adhesive per unit length and can be written as

$$K_{n2} = \frac{\sigma_n(x)}{\Delta w(x)} = \frac{E_{a2}}{t_{a2}} \tag{16}$$

The general solution to this fourth-order differential equation is

$$\sigma_n(x) = e^{-\phi x} \left[\eta_9 \cos(\phi x) + \eta_{10} \sin(\phi x) \right] + e^{\phi x} \left[\eta_{11} \cos(\phi x) + \eta_{12} \sin(\phi x) \right] - \left(\frac{y_2 b_3 - \frac{D_{11}^{'} E_2 I_2 t_3}{2}}{D_{11}^{'} E_2 I_2 + b_3} \right) \frac{d\tau(x)}{dx} - \frac{1}{D_{11}^{'} E_2 I_2 + b_3} q \tag{17}$$

For large values of x it is assumed that the normal stress approaches zero and, as a result, $\eta_{11}=\eta_{12}=0$. The general solution therefore becomes

$$\sigma_n(x) = e^{-\phi x} \left[\eta_9 \cos(\phi x) + \eta_{10} \sin(\phi x) \right] - \left(\frac{y_2 b_3 - \frac{D_{11}^{'} E_2 I_2 t_3}{2}}{D_{11}^{'} E_2 I_2 + b_3} \right) \frac{d\tau(x)}{dx} - \frac{1}{D_{11}^{'} E_2 I_2 + b_3} q \tag{18}$$

Where:

$$\phi = \left[\frac{E_{a2}}{4t_{a2}} \left(D_{11}^{'} + \frac{b_3}{E_2 I_2} \right) \right]^{\frac{1}{4}} \tag{19}$$

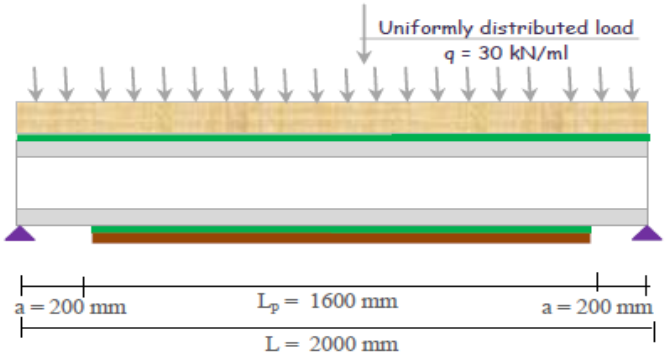

(a) Longitudinal section of aluminum-wood composite beam

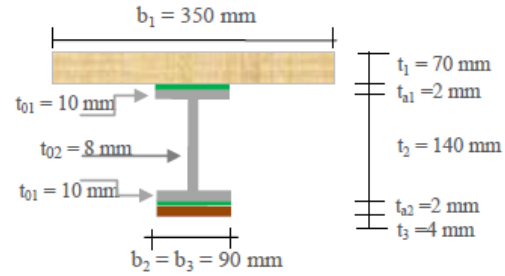

(b) Cross section of aluminum-wood composite beam: section of Aluminum I-beam

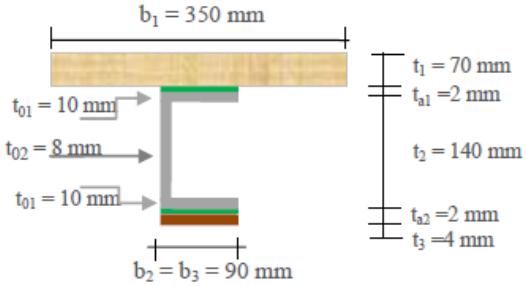

(c) Cross section of aluminum-wood composite beam: section of Aluminum U-shaped beam

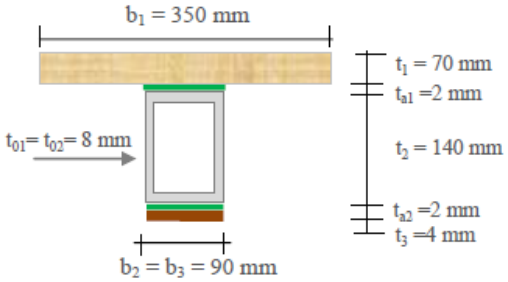

(d) Cross section of the aluminum-wood composite beam: section of rectangular aluminum tube beam

Figure 5. Composite aluminum-wood beam strengthened by composite plate: geometric characteristic

As is described by Hassaine Daouadji [27], the constants η_9 and η_{10} in Eq. (17) are determined using the appropriate boundary conditions and they are written as follows:

Table 1. Geometric and mechanical properties of the materials used

Component	Width (mm)	Depth (mm)	Young's modulus (MPa)	Poisson's ratio
Adhesive layer	b_a=80	t_a=2	E_a=128000	0.35
Fiber Carbone HR	b_3=80	t_3=4	E_3=140 000	0.28
Aluminum Beam	b_2=80	t_2=200	E_2=65300	0.3

Table 2. Mechanical properties of the materials used in construction wood from Algerian forests

Material property	Use of wood products in civil construction from El Ouarsenis forests Algerian		
	Eucalyptus wood from the forest of Bordj BouNaama	Aleppo pine wood from the forest of Tiaret	Cedar wood from the Théniat el Had forest
Young's modulus (MPa)	12000	14000	16000
Poisson's ratio	0.22	0.24	0.24
Volume Weight (kg/m^3)	490	650	590

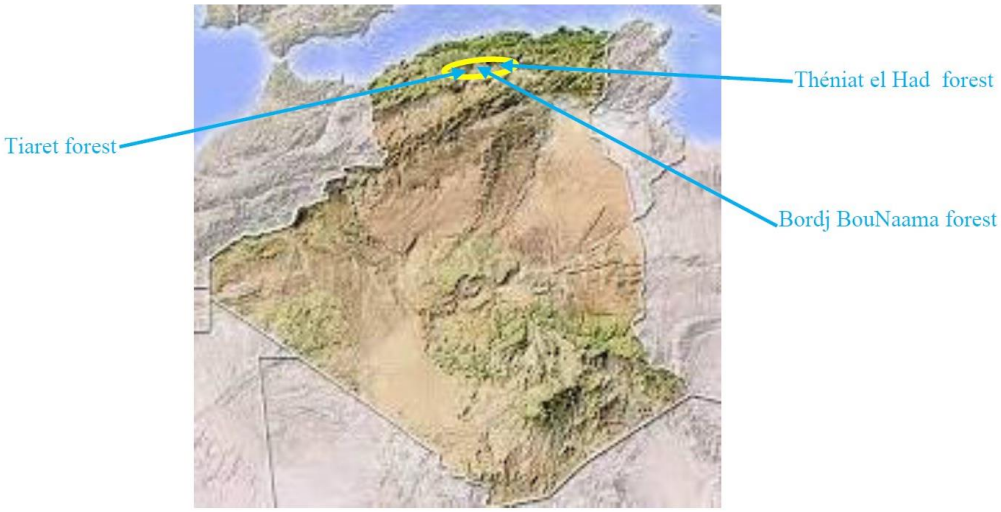

Photo 01: El Ouarsenis forests area affected by timber extraction from the western Algerian highlands

$$\eta_9 = \frac{K_{n2}\left[V_T(0) + \phi M_T(0)\right]}{2\phi^3 E_2 I_2} - \frac{b_3 K_{n2}\left(\frac{y_2}{E_2 I_2} - \frac{D_{11}' t_3}{2b_3}\right)}{2\phi^3}\tau(0) + \frac{\left[\frac{d^4\tau(0)}{dx^4} + \phi\frac{d^3\tau(0)}{dx^3}\right]}{2\phi^3} \tag{20}$$

$$\eta_{10} = -\frac{K_{n2}}{2\sqrt{\frac{K_{n2}}{4}\left(D_{11}' + \frac{b_3}{E_2 I_2}\right).E_2 I_2}} M_T(0) - \frac{y_2 b_3 - \frac{D_{11}' E_2 I_2 t_3}{2}}{2\sqrt{\frac{K_{n2}}{4}\left(D_{11}' + \frac{b_3}{E_2 I_2}\right)}} \frac{d^3\tau(0)}{dx^3} \tag{21}$$

The above expressions for the constants η_9 and η_{10} has been left in terms of the bending moment $M_T(0)$ and shear force $V_T(0)$ at the end of the soffit plate. With the constants η_9 and η_{10} determined, the interfacial normal stress can then be found using Eq. (17).


Photo 02: Eucalyptus wood from the forest of Bordj BouNaama


Photo 03: Aleppo pine wood from the forest of Tiaret


Photo 04: Cedar wood from the Theniat el Had forest

3. Results and analysis

3.1 Material used in this study

A computer code developed to calculate interfacial stresses in a composite aluminum -wooden beam, subjected to both uniformly distributed and concentrated loads. The geometric and material properties of the beam summarized in Fig. 5, Tables 1 and 2, and illustrate its dimensions. The study subjects come from the forests of the western Algerian highlands (photo 01), such as the Tiaret (photo 03) region, Bordj BouNaama (photo 02) and Theniat el Had (photo 04).

Table 3. Comparison interfacial stress with analytical model for composite aluminum-wood beam strengthened by sika wrap

Comparison interfacial stress with analytical model for composite aluminum-wood beam strengthened by sika wrap						
	Cedar Wood		Eucalyptus wood		Aleppo Pine Wood	
Interfacial stress	τ(x)	σ(x)	τ(x)	σ(x)	τ(x)	σ(x)
Present model	6,4266	3,3594	6,4094	3,3505	6,42978	3,36113
Hassaine Daouadji [2]	6,8311	3,7842	6,8179	3,7735	6,8422	3,7951

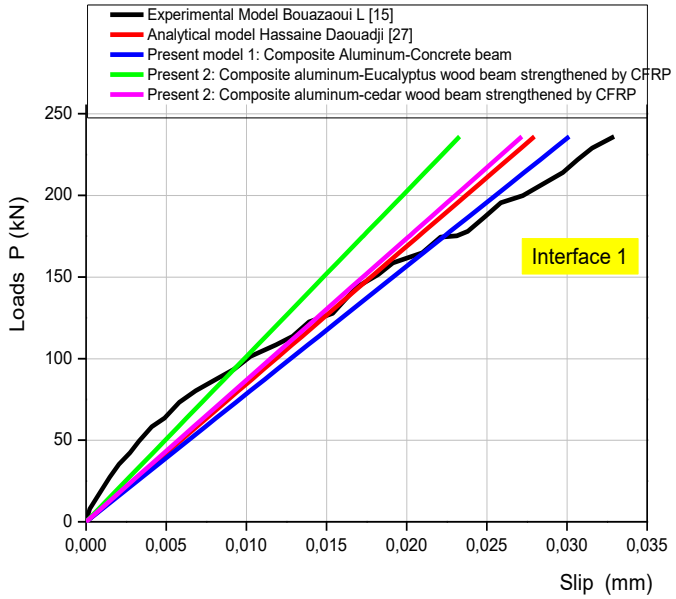

Figure 6. Load-slip curves of composite aluminum-wood beam strengthened by CFRP: Experimental and analytical comparison of results

3.2 Validation of analytical model

The study validates an analytical model for a composite aluminum-wood beam strengthened with a composite plate by comparing slip results (Fig. 6). with experimental data from Bouazaoui [15] and Hassaine Daouadji [27]. The results show good agreement, confirming the new model's validity. The study emphasizes the importance of using a reinforced composite plate for better slip control.

The study examines the impact of adherend shear deformations on maximum shear and normal stress using parabolic shear stress distribution across the thickness of adherends. It compares the results (Table 3) with the current theory and Hassaine daouadji's [2] theory, which assumes linear shear stress through the thickness of adherends. Results show that adherend shear deformation reduces interfacial stresses concentration, making the adhesive shear distribution more uniform. The interfacial normal stress changes sign at a short distance away from the plate end, confirming the predictions of the different solutions.

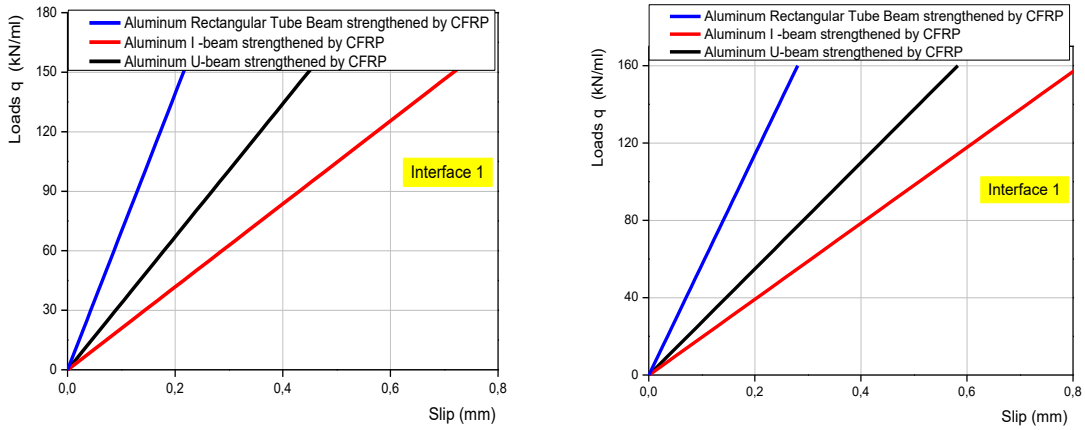

(a) Composite aluminum- Eucalyptus wood beam (b) Composite aluminum- Cedar wood beam

Figure 7. Effect of the geometry of the Aluminum beam of composite aluminum- wooden beam strengthened by CFRP "Interface 1"

Table 4. Effect of geometry for composite I-Aluminum-wooden beam reinforced by 4-ply fabric (sikawrap) "Interface 2"

Effect of geometry for composite Aluminum-wooden beam reinforced by 4-ply fabric (sikawrap)				
Cross section of aluminum-wood composite beam	Stress	Cedar Wood	Eucalyptus wood	Aleppo Pine Wood
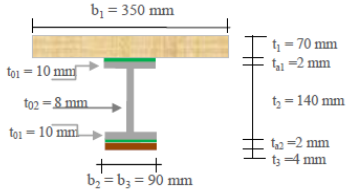	τ(x)	6,9123	6,8945	6,9245
	σ(x)	3,6233	3,6234	3,6356
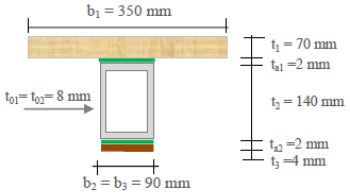	τ(x)	6,6174	6,5997	6,6207
	σ(x)	3,4726	3,4633	3,4743
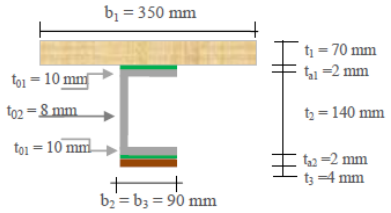	τ(x)	6,9086	6,8901	6,9120
	σ(x)	3,61114	3,6017	3,6132

3.3 Parametric studies

The study aimed to understand the behavior of bonded composite aluminum beam-wooden slab repairs through a parametric study program, utilizing an analytical approach to optimize design

parameters and investigate the effects of various parameters.

3.3.1 Effect of Aluminum beam geometry:

The numerical results of this solution study the impact of slip distributions on an aluminum beam of a composite aluminum-wooden beam strengthened by CFRP, considering the stiffness of the wooden slab on the slip.

- The three types of aluminum beam geometry: rectangular tube, I-shape, and U-shape
- The two types of wood: cedar wood from the Theniat el Had forest and eucalyptus wood from the Bordj Bou Naama forest.

These results aim to demonstrate the main characteristics of the slip distributions in these composite beams. The numerical results are presented in Fig. 7 (a) and (b). The effect of the load on interfacial slip is illustrated. The current analytical model in the elastic domain shows good agreement between the curves, confirming the validation of the new model. It was also observed that slip was maximum without the use of the CFRP plate in the aluminum-wood composite beam and minimum with the use of this CFRP plate. It was noted that the beam with the stiffest geometry, with a double web (case of the rectangular and U-shaped beam), slip becomes low compared to the I-shaped section. Similarly, for the wooden slab, it is clear that the stiffest wood presents stability.

The numerical results of a study examine the impact of the stiffness of a sikawrap-strengthened aluminum-wooden composite beam on the distribution of shear and interface normal stresses in the aluminum composite beam (Table 4), while maintaining the same mechanical parameters.

- The three types of aluminum beam geometry: rectangular tube, I-shape, and U-shape
- The three types of wood: cedar wood from the Theniat el Had forest and eucalyptus wood from the Bordj Bou Naama forest and Aleppo pine wood from the forest of Tiaret.

The study reveals that as the plate material becomes softer and the wooden slab's stiffness increases, interfacial stresses decrease from the stiffest to the least stiff section. This is due to lower tensile force and reduced interfacial stresses, with the peak interfacial shear stress moving closer to the free edge.

3.3.2 Effect of adhesive thickness: Aluminum I-beam case

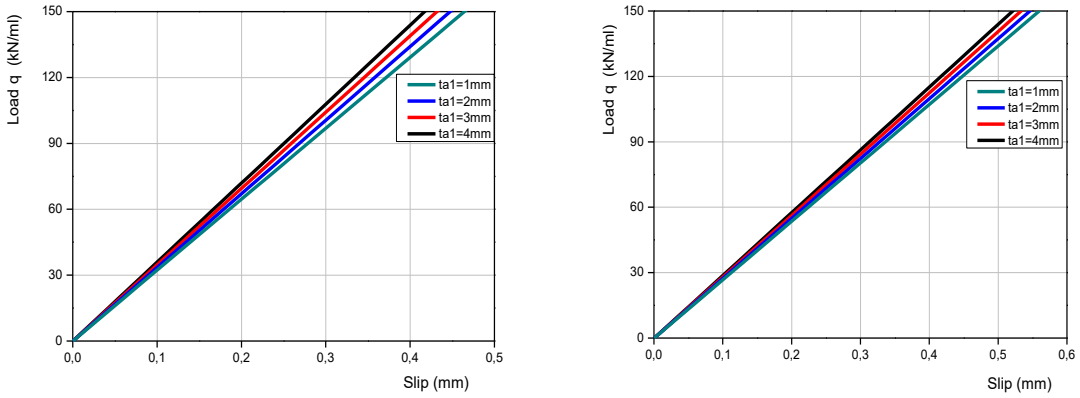

(a) Composite aluminum-Eucalyptus wood beam (b) Composite aluminum-Cedar wood beam

Figure 8. Effect of adhesive thickness of Composite aluminum- wooden beam "Interface 1"

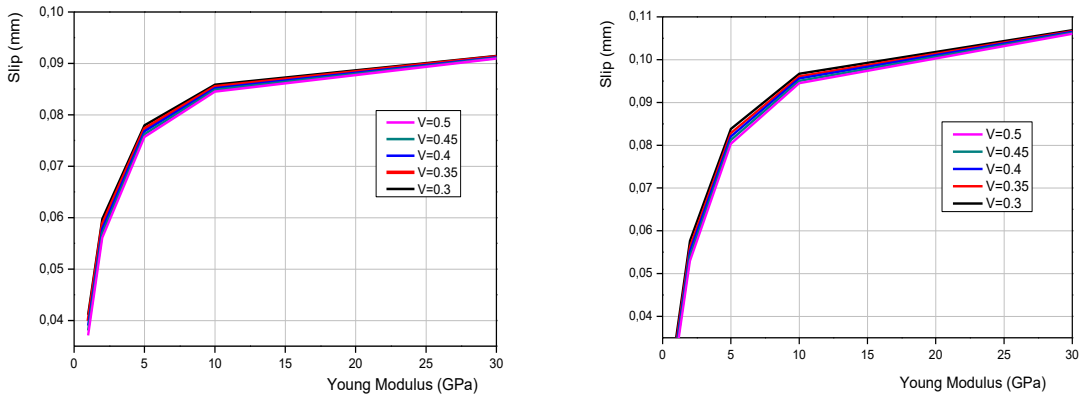

(a) Composite aluminum-Eucalyptus wood beam (b) Composite aluminum-Cedar wood beam

Figure 9. Effect of Young's modulus adhesive of Composite aluminum- wooden beam "Interface 1"

Fig. 8 (a) and (b) (interface 1) illustrate the effect of adhesive layer thickness t_{a1} on the beam's sliding and interfacial stresses. Effect of adhesive thickness of composite aluminum-wooden beam strengthened by Sika wrap. The thickness of the adhesive layer significantly reduces maximum interfacial stresses, making it recommended to use a thick layer at the edges to prevent the Sika wrap plate from detaching. However, a thin layer is strongly advised to prevent the wooden slab from sliding and secure it to the aluminum beam.

3.3.3 Effect of Young's modulus of adhesive: Aluminum I-beam case

For Interface 1: To analyze the effect of Young's modulus of adhesive on the aluminum-wooden composite beam "Interface 1", we used the following materials:

- An I-shaped aluminum beam.
- Two types of wood: cedar wood from the Theniat el Had forest and eucalyptus wood from the Bordj Bou Naama forest.

Fig. 9 (a) and (b) illustrate the influence of the adhesive's modulus of adhesion for different Poisson's ratios (v=0.3, v=0.35, v=0.4, v=0.45, and v=0.5) on the sliding of the aluminum-wooden composite beam. It is clear that the higher the Poisson's ratio, the greater the sliding; however, the higher the Young's modulus of the adhesive, the lower the sliding. Therefore, it is recommended to use an adhesive with a sufficient Young's modulus.

4. Conclusions

An advanced theoretical method was employed to analyze interfacial stresses within composite aluminum-wood beams that have been reinforced with Sika Wrap. The study incorporated shear strains of the bonds, assuming that these strains follow nonlinear distributions across the thickness of the bond. This methodological advancement aids in comprehending the cooperative behavior of composite beams and in formulating adequate design guidelines for their utilization. Traditional methodologies tend to underestimate bond stress distributions and peak interfacial stresses; however, the new approach yields accurate predictions for the interface stresses located at both the upper and lower surfaces of the aluminum beam. Furthermore, extensive parametric studies were

carried out using this new solution, specifically focusing on beams that had been strengthened with varying design parameters. The effectiveness of the new method was successfully validated through experimentation, where a previously existing discontinuous connection was supplanted with a novel continuous connection facilitated by the adhesive. This innovation aims to minimize slippage between the aluminum and wood bonds by enhancing their adhesion and stability, which aligns with the primary goal of the research. Importantly, the newly developed solution is versatile and can be adapted to various materials, with significant implications for civil construction applications.

References

1. Tounsi, A. (2006). Improved theoretical solution for interfacial stresses in concrete beams strengthened with FRP plate. International Journal of Solids and Structures, 43(14-15), 4154-4174. https://doi.org/10.1016/j.ijsolstr.2005.03.074.
2. Tahar, H.D., Boussad, A., Abderezak, R., Rabia, B., Fazilay, A., Belkacem, A. (2019). Flexural behaviour of steel beams reinforced by carbon fibre reinforced polymer: experimental and numerical study. Structural Engineering and Mechanics, 72(4), 409-420. https://doi.org/10.12989/sem.2019.72.4.409.
3. Benachour, A., Benyoucef, S., Tounsi, A. (2008). Interfacial stress analysis of steel beams reinforced with bonded prestressed FRP plate. Engineering Structures, 30(11), 3305-3315. https://doi.org/10.1016/j.engstruct.2008.05.007.
4. Daouadji, T.H. (2013). Analytical analysis of the interfacial stress in damaged reinforced concrete beams strengthened by bonded composite plates. Strength of Materials, 45(5), 587-597. https://doi.org/10.1007/s11223-013-9496-4.
5. Rabia, B., Daouadji, T.H., Abderezak, R. (2023). Mechanical behavior of RC beams bonded with thin porous FGM plates: case of fiber concretes based on local materials from the mountains of the Tiaret highlands. Coupled Systems Mechanics, 12(3), 241-260. https://doi.org/10.12989/csm.2023.12.3.241.
6. Daouadji, T.H. (2017). Analytical and numerical modeling of interfacial stresses in beams bonded with a thin plate. Advances in Computational Design, 2(1), 57-69. https://doi.org/10.12989/acd.2017.2.1.057.
7. Tayeb, B., Abderezak, R., Daouadji, T.H. (2024). Mechanical behavior of composite beam aluminum-sandwich honeycomb strengthened by imperfect FGM plate under thermo-mechanical loading. Coupled Systems Mechanics, 13(2), 133-151. https://doi.org/10.12989/csm.2024.13.2.133.
8. Tounsi, A., Daouadji, T.H., Benyoucef, S. (2009). Interfacial stresses in FRP-plated RC beams: Effect of adherend shear deformations. International Journal of Adhesion and Adhesives, 29(4), 343-351. https://doi.org/10.1016/j.ijadhadh.2008.06.008.
9. Baghdadi, M., Bellali, M.A., Campilho, R.D., Serier, B. (2025). Optimization of composite patch designs for enhanced repair efficiency in damaged aircraft structures. Structural Engineering and Mechanics, 94(4), 299-311. https://doi.org/10.12989/sem.2025.94.4.299.
10. Henni, A.H., Daouadji, T.H. (2025). Effect of boundary conditions for functionally graded beams under uniformly distributed load. Coupled Systems Mechanics, 14(3), 231-245. https://doi.org/10.12989/csm.2025.14.3.231.
11. Benferhat, R., Daouadji, T.H., Abbes, B., Bensatallah, T., Rabahi, A., Abbes, F. (2025). Analysis of interfacial stresses of composite bridge box steel-concrete beam. Coupled Systems Mechanics, 14(5), 431-450. https://doi.org/10.12989/csm.2025.14.5.431.
12. Zhang, Y., Wang, Y., Tian, L., Zeng, Y. (2025). Simulation and analysis of composite girders with corrugated steel webs using spatial grid model. Steel and Composite Structures, 55(2), 175-190. https://doi.org/10.12989/scs.2025.55.2.175.
13. Rabia, B., Tahar, H.D., Boussad, A., Tayeb, B., Abderezak, R., Fazilay, A. (2025). Analytical and

numerical study of composite twin-girder bridge decks with adhesive connectors and composite reinforcement. Coupled Systems Mechanics, 14(4), 327-345. https://doi.org/10.12989/csm.2025.14.4.327.
14. Tayeb, B., Daouadji, T.H. (2020). Improved analytical solution for slip and interfacial stress in composite steel-concrete beam bonded with an adhesive. Advances in Materials Research, 9(2), 133-153. https://doi.org/10.12989/amr.2020.9.2.133.
15. Bouazaoui, L., Perrenot, G., Delmas, Y., Li, A. (2007). Experimental study of bonded steel concrete composite structures. Journal of Constructional Steel Research, 63(9), 1268-1278. http://doi.org/10.1016/j.jcsr.2006.11.002.
16. Han, S.J., Kim, M.S., Heo, I., Lee, W.J., Lee, D. (2025). Performances of precast concrete composite double wall systems with discontinuous steel members as shear connector. Steel and Composite Structures, 55(4), 283-295. https://doi.org/10.12989/scs.2025.55.4.283.
17. Ali, Y.A.Z. (2018). Flexural behavior of FRP strengthened concrete-wood composite beams. Ain Shams Engineering Journal, 9(4), 3419-3424. https://doi.org/10.1016/j.asej.2018.06.003.
18. Panjehpour, M., Farzadnia, N., Demirboga, R., Ali, A.A.A. (2016). Behavior of high-strength concrete cylinders repaired with CFRP sheets. Journal of Civil Engineering and Management, 22(1), 56-64. https://doi.org/10.3846/13923730.2014.897965.
19. Kada, D., Abdelouahed, T. (2022). A new refined hyperbolic shear deformation theory for laminated composite spherical shells. Structural Engineering and Mechanics, 84(6), 707-722. https://doi.org/10.12989/sem.2022.84.6.707.
20. Kožar, I. (2024). Analysis of 3D pendulum sliding along a rope. Coupled Systems Mechanics, 13(5), 459-470. https://doi.org/10.12989/csm.2024.13.5.459.
21. Belbachir, N., Tounsi, A., Al-Osta, M.A. (2025). A new HSDT for buckling and free vibration behavior of cross-ply laminated composite plates resting on elastic foundation. Computers and Concrete, 35(1), 29-41. https://doi.org/10.12989/cac.2025.35.1.029.
22. Chen, B.L., Gao, H.Y., Wang, L.G. (2024). Experimental study on hollow GFRP-confined reinforced concrete columns under eccentric loading. Steel and Composite Structures, 52(4), 451-460. https://doi.org/10.12989/scs.2024.52.4.451.
23. Bousmaha, K., Belalia, S.A., Chorfi, S.M., Tounsi, A., Al-Osta, M.A., Alluqmani, A.E. (2025). On the dynamic behavior of plates made of porous advanced materials reinforced with carbon nanotubes using ap-version of finite element method. Mechanics Based Design of Structures and Machines, 1-30. https://doi.org/10.1080/15397734.2025.2534679.
24. Saini, K., Lalthazuala, R., Singh, T.G. (2025). Flexural behaviour of hybrid high-strength steel I-beams. Steel and Composite Structures, 55(4), 319-332. https://doi.org/10.12989/scs.2025.55.4.319.
25. Becheur, A., Coorevits, P. (2025). Numerical investigations of contact behavior in beam to column end plate connections. Structural Engineering and Mechanics, 94(5), 375-383. https://doi.org/10.12989/sem.2025.94.5.375.
26. Henni, A.H., Daouadji, T.H. (2025). Application of a new improved Airy polynomial function for FGM cantilever beams under concentrated load. Coupled Systems Mechanics, 14(2), 161-173. https://doi.org/10.12989/csm.2025.14.2.161.
27. Daouadji, T.H., Abbès, B., Bensatallah, T., Abbès, F. (2025). Analysis of interface sliding in a composite I-steel–concrete beam reinforced by a composite material plate: the effect of concrete–steel connection modes. Journal of Composites Science, 9(6), 273. https://doi.org/10.3390/jcs9060273.
28. Nguyen, D.D., Ta, H.D., Dao, D.S., Nguyen, H.D. (2025). Column buckling under stochastic three-dimensional material properties: A stochastic finite element analysis. Coupled Systems Mechanics, 14(4), 347-369. https://doi.org/10.12989/csm.2025.14.4.347.
29. Mataich, H. (2025). Parametric dynamic instability of a suspension bridge deck under dynamic loading along two of its opposite edges. Coupled Systems Mechanics, 14(3), 269-288. https://doi.org/10.12989/csm.2025.14.3.269.
30. Mataich, H., El Amrani, A., El Amrani, B. (2024). Analysis of the thermal instability of laminated composite plates. Coupled Systems Mechanics, 95-113. https://doi.org/10.12989/csm.2024.13.2.095.